1-20-2006

Multi-Reference Pseudo-Random Phase-Encoded Joint Transfrom Correlation

Edward Mwatibo
University of New Orleans

MULTI-REFERENCE PSEUDO-RANDOM PHASE-ENCODED JOINT TRANSFORM CORRELATION

A Thesis

Submitted to the Graduate Faculty of the
University of New Orleans
in partial fulfillment of the
requirements for the degree of

Master of Science
in
Engineering

by

Edward Mwatibo

M.S. University of New Orleans, 2005

December 2005

DEDICATION

I give my sincere love and thanks to my whole family especially my dear wife and my children, for their endless love, unlimited caring, and understanding. I also highly appreciate the help extended by my colleagues and friends. Your support and encouragement often inspired me.

ACKNOWLEDGMENTS

I would first like to express my gratitude to my advisor, Dr. Abdul Rahman Alsamman, for giving me this opportunity to study with him. I appreciate his insightful guidance, patience, encouragement, understanding and support during this research. I would also like to thank the other members of my committee, Dr. Dimitrios Charalampidis and Mr. Kim Jovanovich, for the assistance they provided at all levels of the research project.

TABLE OF CONTENTS

LIST OF FIGURES

LIST OF TABLES

ABSTRACT

We propose and demonstrate the superiority of using a phase SLM only in a multi-reference phase encoded joint transform correlator(JTC) compared to an ordinary JTC. Maximal length sequences are shifted to form two dimensional orthogonal arrays referred as m-arrays. The phase mask is used in one step to encode multiple reference images and at the same time eliminate false correlation peaks through power spectrum dispersion. A theoretical model of the implemented JTC is mathematically expressed and explained in this thesis. Basic performance criteria, PSR (peak to side lobe ratio) and PCE (peak to correlation energy), are used for comparative analysis, and their relationship to joint input image size and SLM size are investigated and the results simulated.

1 INTRODUCTION

The development of optical components during the twentieth century has led to many advances in the design of optical processing systems, which are used as data processing systems and to complement computerized systems. The popularity of optical processing is mainly due to their processing capabilities and immense parallelism.

Fourier optical signal processing is one of the oldest forms of optical signal processing, with a history dating back to 1893 [1]. Its foundation is based on the ability of a lens to perform two-dimensional (2D) Fourier transform. Since their introduction, optical processing systems have successfully been utilized in a variety of areas including radar signal processing, optical pattern recognition and target tracking.

There are two commonly used optical correlation techniques: The first is matched spatial filtering optical correlation, developed by Vander Lugt [2] in 1964, and the second is the joint transform correlation (JTC) proposed by Weaver and Goodman [3] in 1966. For real time applications, JTC is preferred over Vander Lugt correlator because it does not require complex filtering or precise alignment, but it suffers strong zero order term and has overlapping correlation peaks. To reduce these effects, an increase in displacement between the images is required or an optical stop is introduced at the center of the output plane, thus leading to a more inefficient use of the spatial area of the optical beam.

Different architectures [4] have since been proposed to improve the JTC optical correlators in performance and discrimination ability, especially in the presence of multiple input images. These architectures include techniques that involve nonlinear algorithms which adjust the joint power spectrum

(JPS), like binary JTC [5], amplitude-modulated filter based JTC [6], and chip-encoded JTC [7] and fringe-adjusted JTC [8]. Other methods that have been implemented to improve correlation discrimination by reducing extraneous peaks include Fourier plane image subtraction [9] and phase encoding input JTC technique [10, 11]. These systems are considerably more complex in design. None of the proposed techniques in literature have attempted to improve the spatial inefficiency of the JTC system.

1.1 PROBLEM DESCRIPTION

In this thesis, we introduce a phase encoded JTC system that employs Pseudo-random phase masks to encode multiple reference images in a JTC system. The phase masks are generated using maximal length sequences (M-sequences), which are Pseudo-random sequences that are easy to generate and have low autocorrelation and cross correlation side lobes. The system will be designed to make exploit the parallelism inherent in the optical system and to multiplexing many reference images in phase such that multiple correlations can be performed at the same time. A reference-encoding method will be utilized to considerably simplify the architecture of the proposed system. The random phase mask is used to improve the spatial efficiency by eliminating the spatial displacement between the input and reference images. The actual phase encoding process is performed electronically *a prior* thus removing the need for online encoding.

1.2 THESIS ORGANIZATION

Chapter 2 provides a brief overview of optical processing and its advantages. It also includes a summary of the main optical components and a description of the variant JTC architecture. Chapter 3 presents a general theory of Pseudo-random sequences and reviews the major approaches that have

been used to create two-dimensional M-sequence arrays used for phase-encoding. Chapter 4 describes the implementation details for the modified phase encoded JTC and investigates the effect of image size and SLM size on the correlation output. Chapter 5 presents computer simulated results of the proposed system. Finally, Chapter 6 concludes the thesis by summarizing the major results, analyzing some of the minor problems encountered and discussing areas that could be improved in future work.

2 OPTICAL PROCESSING

Compared to their electronic counterparts, optical system possess: a higher degree of parallelism, a faster processing speed that is more suited for real time applications, immune to electromagnet interference, and provide low-loss transmission with large bandwidth[12].

2.1 BASIC OPTICAL COMPONENTS

A vast development in optoelectronic devices in the last century has enabled the creation of optical data processors. These devices are the fundamental key in the integration between electronics and optical technology. Table 2-1 groups different optical components into four major categories: signal generators, signal modulators, signal detectors and signal steering devices.

Category	**Device**
Signal Generator	LED (Light emitting diode) VCSEL(Vertical cavity surface emitting laser)
Signal Modulator	LCD (Liquid crystal display) AOSLM (Acousto optic spatial light modulator) EOLM (Electro optical light modulator)
Signal Detector	CCD (Charged coupled device) CMOS (Complementary metal-oxide semiconductor) detector
Signal Steering Device	Mirrors Prisms Lenses

Table 2-1: Examples of Opto-electronic Devices

All four categories (generation, modulation, steering and detection) are operative in the joint transform correlation process.

- Signal generators

  Light sources, which come in a huge array of sizes, shapes, and colors, are selected depending on response speed required, bandwidth to be achieved and the type of application to be used in. In optical processing, Laser diodes and LED (light emitting diodes) are the main types of lighting sources used.

- Signal modulators: these devices are also known as spatial light modulators (SLMs).

  The SLM is an opto-electronic input device that plays an important role in an optical processing system by controlling light on a pixel-to-pixel basis. The SLM accepts the input data (pattern information) from a digital input (host computer) and converts coherent light input from a laser source into output data. Commercially, SLMs are classified using the following criteria [13]: addressing methods; coherent light requirement; modulation scheme; quality of the input; setup and hold time; other specifications include size, power consumption and range of temperature. For a phase-only mode, the SLM encodes the input light beam with a phase such that it produces the desired input data, which can be expressed as

  $$A(r) = A_0(r)e^{iy(r)} \qquad (1)$$

  where $A_0(r)$ is the complex amplitude of the beam incident on the SLM [14].

  Although the use of SLMs increases the overall flexibility, they have the following disadvantages; high cost, performance limitation, and design issues such as phase uniformity and contrast ratios.

The most commonly used SLM types are Liquid Crystal Television (LCTV), Magneto-optic SLM (MOSLM), and Deformable Mirror Device (DMD) [15].

- Signal steering devices

1. Mirrors

   Optical beam steering is commonly accomplished via the use of mirrors and prisms. This kind of combination tends to increase the size, weight and complexity of the optical system. Mirrors and prisms control direction of light through reflection and refraction respectively.

2. Beam Splitters (BS)

   Beam splitter is an optical device that is used to split a beam of light into two or more light beams. It consists of partially transparent mirror (half–silvered) which allows part of the beam light to reflect off while the other part goes through it. It is also referred to as Beam Combiner when used to combine multiple beams into a single beam.

3. Lenses

   Optical signal processing has relied heavily on the Fourier transform property of a lens, which was discovered a century ago by German scientist E. Abbe [16]. Both the 2 D Fourier and its inverse transform are performed by a converging lens, which also captures as much of the source light beam as possible and transforms it into a collimated output.

- Signal detectors

  Charged Coupled Device (CCD) Detector

  W.S. Boyle and G.E. Smith of the Bell Laboratory [17] invented the Charged Coupled Device (CCD) known as a square–law device in 1969. This device, which converts incident light into photoelectrons, has gained a widespread application in both scientific and commercial imaging.

The interface between the optical and electronic system in a JTC is provided by a combination use of SLMs and CCDs. This opto-electronic interaction forms the basis of hybrid operation, enabling an optimal achievement in terms of performance, speed and cost.

2.2 MATCHED FILTER CORRELATOR

The fundamental theory of optical spatial filtering was introduced by Cheatham, Kohlenberg and O'Nell [18]. Since then significant progress has been made in spatial filtering with Vander Lugt [2] presenting an optical correlator using complex spatial filtering 1964. His system performed a correlation between two functions $f(x,y)$ and $h(x,y)$ and is based on the correlation theorem and the Fourier transform property of a lens and coherent light.

The correlation theorem states that convolution operation between two functions $f(x,y)$ and $h(x,y)$ in the spatial domain is equivalent to a simple multiplication in frequency domain.

$$F(u,v) = \Im\{ f(x,y) \otimes h(x,y)\} = F(u,v)H(u,v) \tag{2}$$

where $\otimes$ is a symbol for convolution operation.

Figure 2-1 shows a matched based correlator that utilizes the correlation property to perform the correlation between two images. This type of correlator requires *a priori* fabrication of the complex valued matched filter and initial transformation of the reference image.

Correlation output $C(x,y)$ is obtained when the system is online

$$C(x,y) = \Im^{-1}\left\{F(u,v)H^{*}(u,v)\right\} \tag{3}$$

where $\Im^{-1}$ stands for inverse Fourier transformation, $F(u,v)$ and $H(u,v)$ are Fourier transform of

$f(x,y)$ and $h(x,y)$ performed optically and multiplied together. $H^*(u,v)$ is a complex conjugate function expressed in terms of magnitude and phase and represents a matched filter.

$$H(u,v) = |H(u,v)|.e^{if(u,v)} \quad (4)$$

Through CCD1, the input scene is captured and uploaded to SLM1 by the switching interface while lens L1 collimates the coherent light provided by the light source LS. The image loaded on SLM1 is modulated onto the beam and Fourier transformed by lens L1 while the prior computed matched filter is loaded on SLM2 through the switching interface.

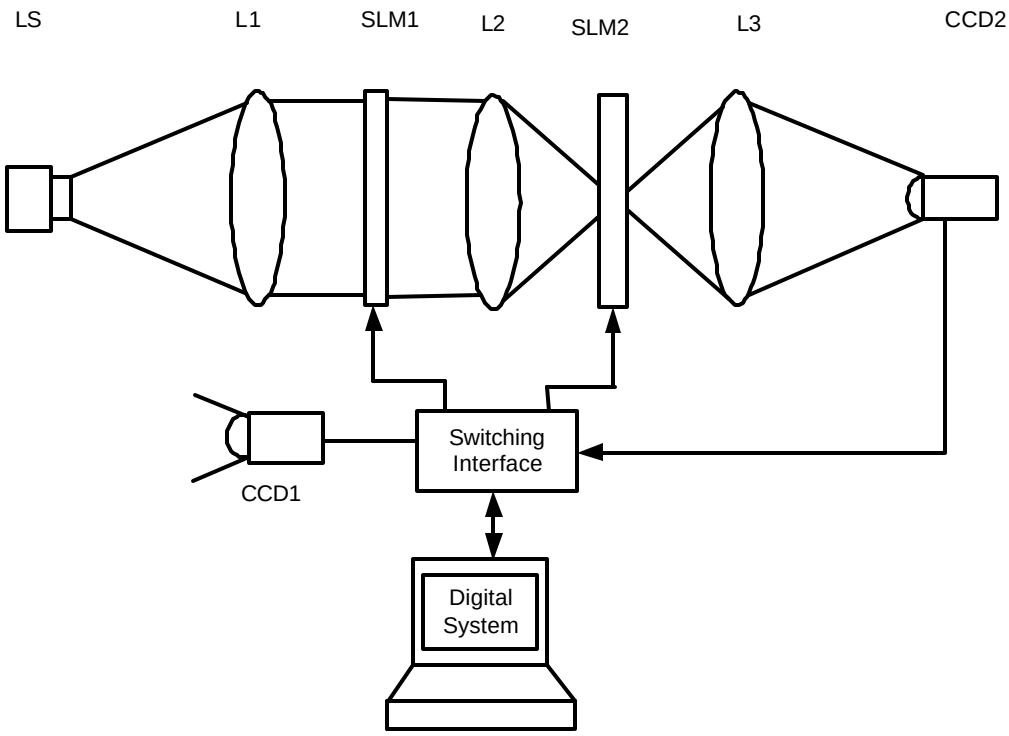

Figure 2-1: A Matched Filter based Correlator

Although the matched spatial filter produces the highest signal-to-noise ratio in the image plane [19], there exist several disadvantages to its use in practice:

1) It requires *a priori* fabrication of a complex matched filter used in the Fourier plane.

2) It requires accurate alignment along the optical axis and close positioning between the filter and the Fourier transform of the input.

3) It is difficult to implement in real time.

4) It requires a second SLM to display phase information, thus an extra cost.

In an effort to improve the spatial filter based correlator, Vander lugt [20] and Cai [21] studied the effects of misalignment of optical setup, while Montes-Usategui [22] presented an automated iterative process to correct some of the misalignment that occurs during operations. Davis [23] and Juvells [24] used divergent lens and photographic teleobjective respectively between the scene and the filter in an attempt to reduce the correlation setup size.

2.3 JOINT TRANSFORM CORRELATOR

Weaver and Goodman [3] originally proposed the joint transform correlator (JTC) for optically convolving two functions. This technique has shown remarkable promise for real-time applications like optical pattern recognition and tracking application. A JTC can be summarized as a two-staged Fourier transform operation attained on the simple principle of a lens focusing a beam of coherent light that has been modulated with images [3]. To explain the basic theory of optical correlation, a simplified JTC is setup up as shown in Figure 2-2. In this approach, light from a coherent source LS is collimated by lens L1 onto input plane SLM1.

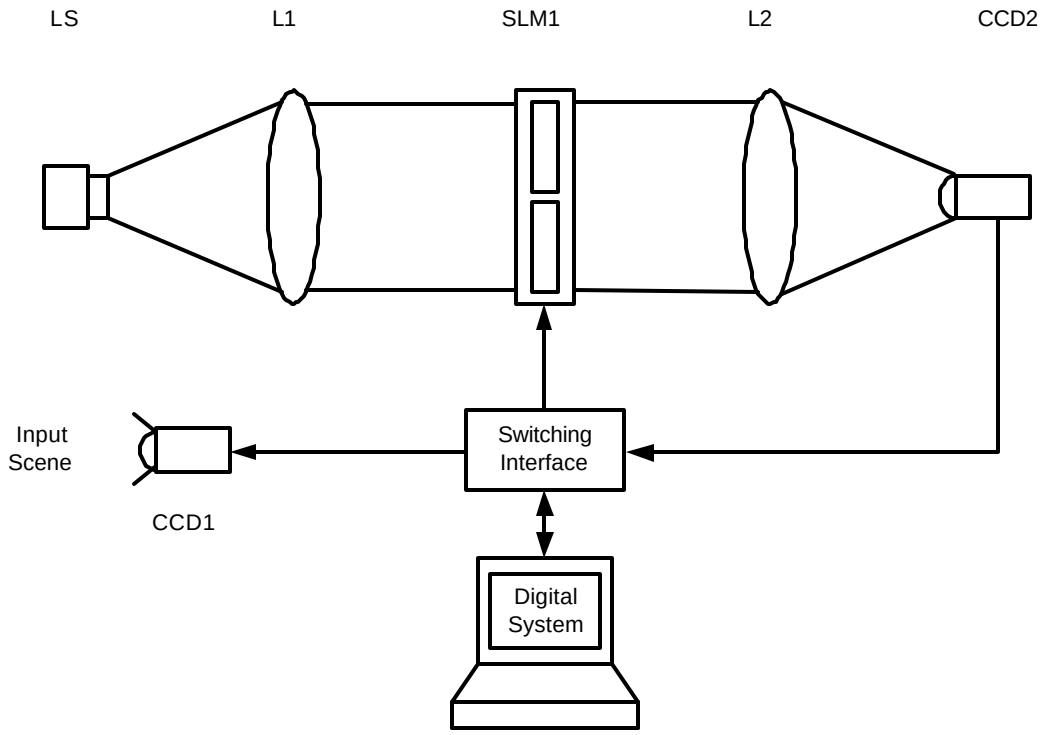

Figure 2-2: Joint Transform Correlator

On SLM1, both the input target image $t(x,y)$ captured using CCD1 and the reference image $r(x,y)$ downloaded from the digital system are placed side to side with a separation (y on both sides) as expressed in the following equation:

$$f(x,y) = r(x, y - y_0) + t(x, y + y_0) \tag{5}$$

A physical separation (2 y) between the reference object and the target object is required (as shown in Figure 2-3) because of the existence of zero-order spectra. This requirement hampers the utilization efficiency of the input spatial domain and lowers the diffraction efficiency of the correlation peaks. Lens L2 Fourier transforms the input joint input image $f(x,y)$ to form

$$\begin{aligned} F(u,v) &= \Im\{ f(x,y)\} = T(u,v)\exp[-jyv] + R(u,v)\exp[-jyv] \\ &= |R(u,v)| \exp[f_r(u,v)]\exp[jy_0v] + |T(u,v)|\exp[f_t(u,v)]\exp[-jy_0v] \end{aligned} \tag{6}$$

where $|R(u,v)|$ and $|T(u,v)|$ represent the magnitude while $f_r(u,v)$ and $f_t(u,v)$ are the phases for the reference and target images respectively. The frequency-domain variables are mutually independent and are represented by u and v.

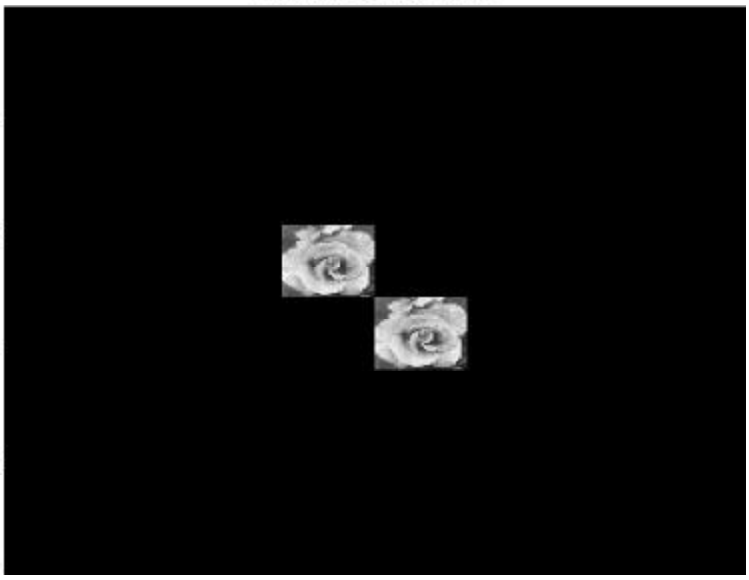

Figure 2-3: Joint Input Image

The Joint Power Spectrum (JPS) which defines the intensity of the Fourier Transform is captured by a square law detector CCD2, and is expressed mathematically as

$$\begin{aligned} G(u,v) &= |F(u,v)|^2 \\ &= |R(u,v)|^2 + |T(u,v)|^2 + 2|R(u,v)|^2 |T(u,v)|^2 \times \cos[f_r(u,v) - f_t(u,v) + 2vy_0] \end{aligned} \quad (7)$$

To obtain the final correlation output $c(x,y)$, the JPS is inversely Fourier Transformed as shown in Figure 2-4, giving the following equation

$$\begin{aligned} C(x,y) &= r(x,y) \otimes r^*(x,y) + t(x,y) \otimes t^*(x,y) \\ &+ r(x,y-2y) \otimes t^*(x,y-2y) + r^*(x,y+2y) \otimes t(x,y+2y) \end{aligned} \quad (8)$$

where $C_{rr}(x,y)$: Autocorrelation of the reference image (zero-order), $C_{tt}(x,y)$: Autocorrelation of the test image (zero-order), $C_{tr}(x,y-2y)$: Cross correlation of the reference image and the test image located at displacement 2y (first-order), $C_{rt}(x,y+2y)$: Cross correlation of the reference image and the test image located at displacement 2*y* (first-order) and $\otimes$ stands for a correlation operation while * denotes the complex conjugates.

Figure 2-4: Correlation Output

As mention earlier, classical JTC is associated with a high zero order peak, which causes an overlap with the desired cross-correlation whenever there is noise or distortion. In real implementation, zero order peaks cause strong spurious reflections that over saturates the output detector [25]. To alleviate these limitations, a binary JTC is used where the joint power spectrum (JPS) is binarized based on a hard clipping nonlinearity at the Fourier plane to only two values, +1 and -1, before the inverse Fourier transform operation or Fourier plane image subtraction technique is applied.

2.4 FOURIER PLANE IMAGE SUBTRACTION

A Fourier plane image subtraction technique [9] helps eliminate the false alarms that are generated automatically in a JTC when multiple targets or multiple reference objects are present in an input scene. To implement the technique a modified JPS can be obtained by subtracting both the input-scene-only power spectrum $|I(u,v)|^2$ recorded by displaying the input scene at the input plane in the absence of the reference image and the reference-image-only power spectrum $|R(u,v)|^2$ recorded by displaying only the reference image. Since the JPS $|F(u,v)|^2$ is normally recorded by displaying both the reference image and the input scene in the input plane SLM, the modified JPS obtained using the Fourier plane image subtraction technique can be expressed as

$$\begin{aligned} P(u,v) &= |F(u,v)|^2 - |T(u,v)|^2 - |R(u,v)|^2 \\ &= 2\sum_{i=1}^{n} |T_i(u,v)||R(u,v)| \cos\left[f_{tt}(u,v) - f_r(u,v) - ux_i - vy_i - 2vy_0\right] + 2|R(u,v)||N(u,v)| \\ &\quad \times \cos\left[f_r(u,v) - f_n(u,v) - 2vy_0\right] \end{aligned} \tag{9}$$

This equation (9) clearly indicates that the subtraction operation eliminates the false alarms generated by similar input scene images. It also eliminates the cross correlation terms between other objects that are present in the input scene. From the above discussion, we see that Fourier plane image subtraction technique involves multiple processing steps and thus not suitable for real time applications where processing speed is a key factor. Furthermore, it still requires the use of large SLM to accommodate the displacement between the images. The technique can be implemented either optically or electronically.

Figure 2-5 illustrates the architecture of a JTC employing Fourier subtraction technique, where the reference image and test image are loaded on SLM1 from the digital system through the switching

system. Light from light source LS is collimated by lens L1 and passed through SLM1 and SLM2 (phase only SLM), where it is modulated with input information and phase encoded. In the initial operation, the phase only SLM2 is clear, and light passes without being encoded. Beam splitter BS splits the beam of light into two: one through L2 and the other through L3. The Fourier transform of the joint input image is performed by lens L3, captured and downloaded to the digital system by CCD2. An optical stop is setup up on the vertical beam path to block the transmission of reference image and allow only the light modulated with test images pass to L3. In the next operation, SLM2 is set as a phase only SLM representing the negative values while lens L2 performs the inverse Fourier transform which is captured by CCD1 as the correlation output.

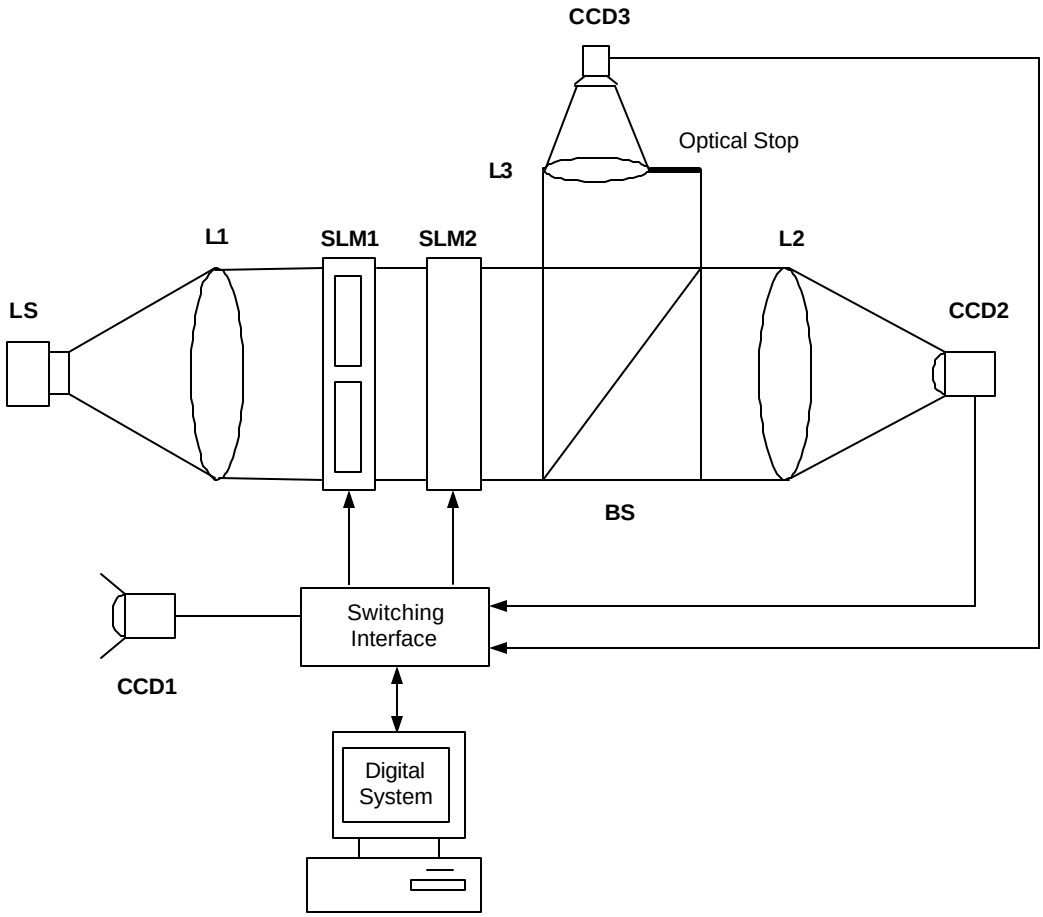

Figure 2-5: JTC Employing Fourier Plane Image Subtraction

2.5 BINARY JTC

Proposed by Javidi and Kuo, [26] binary JTC is superior to classical JTC in terms of correlation peak intensity, correlation width, and discrimination sensitivity [25], but is noted to have lower system processing speed due to the intensive computation required by Fourier plane binarization process. In this process the JPS is binarized into two values (+1 and -1) based on a hardcliping nonlinearity before the inverse transformation process. The threshold for binarization is set by making the histogram of the pixel values of JPS and selecting the median [8].

$$\left|F(u,v)\right|^2 = \begin{cases} +1 & if \left|F(u,v)\right|^2 \geq T \\ -1 & otherwise \end{cases} \tag{10}$$

The architecture of the binary JTC is similar to the architecture of the classic JTC shown in Figure 2-2. The SLM1 is used to display both the input signal and the threshold Fourier transform interference intensity which is the JPS captured by camera CCD2 and binarized by the digital system. The correlation output is computed by the lens L2 and read out at CCD2.

2.6 FRINGE-ADJUSTED JTC

The fringe adjusting technique was proposed by Alam and Karim [8,10] in order to improve coloration discrimination. In this technique, the JPS is multiplied by a real valued filter referred to as FAF (fringe adjusted filter) before applying an inverse Fourier transform to yield the correlation output.

$$H_{FAF(u,v)} = \frac{B(u,v)}{A(u,v) + \left|R(u,v)\right|^2} \tag{11}$$

where $A(u, v)$ and $B(u, v)$ may be constants or functions of v. While $A(u, v)$ is used to overcome the pole and suppress noise, $B(u, v)$ is used to control the optical gain. By multiplying, the JPS With the FAF then the modified JPS mentioned earlier is obtained

$$G(u,v) = \left|F(u,v)\right|^2 \times H_{FAF}$$
$$= B(u,v)\frac{\left|R(u,v)\right|^2 + \left|T(u,v)\right|^2 + \left|R(u,v)\right|\left|T(u,v)\right|\cos\left[f_r(u,v) - f_r(u,v) + 2vy_0\right]}{A(u,v) + \left|R(u,v)\right|^2} \quad (12)$$

when $B(u,v) = 1$ and $\left|R(u,v)\right|^2$ □ $A(v)$ then equation (14) can be simplified as

$$H_{FAF(u,v)} \approx \left|R(u,v)\right|^{-2} \quad (13)$$

and the modified JPS is given by the approximation of equation (12)

$$G(u,v) = 2 + 2\cos\left[f_r(u,v) - f_r(u,v) + 2vy_0\right] \quad (14)$$

Although FJTC suffers from false alarms in the presence of multi-target, it does not require high computations as binary JTC or produce high order harmonics as in a classical JTC [3]. To illustrate the fridge adjusting techniques, the opto-electronic system is setup as in

Figure 2-6. In this fringe-adjusted architecture, the SLM2 is initial set to a transparent mode to allow CCD2 to capture the JPS. On the next operation, SLM2 is loaded with the fridge-adjusted filter from the digital system. Lens 2 performs inverse Fourier transform of product of input image and the corresponding captured JPS. CCD2 captures the correlation output and download to the digital system.

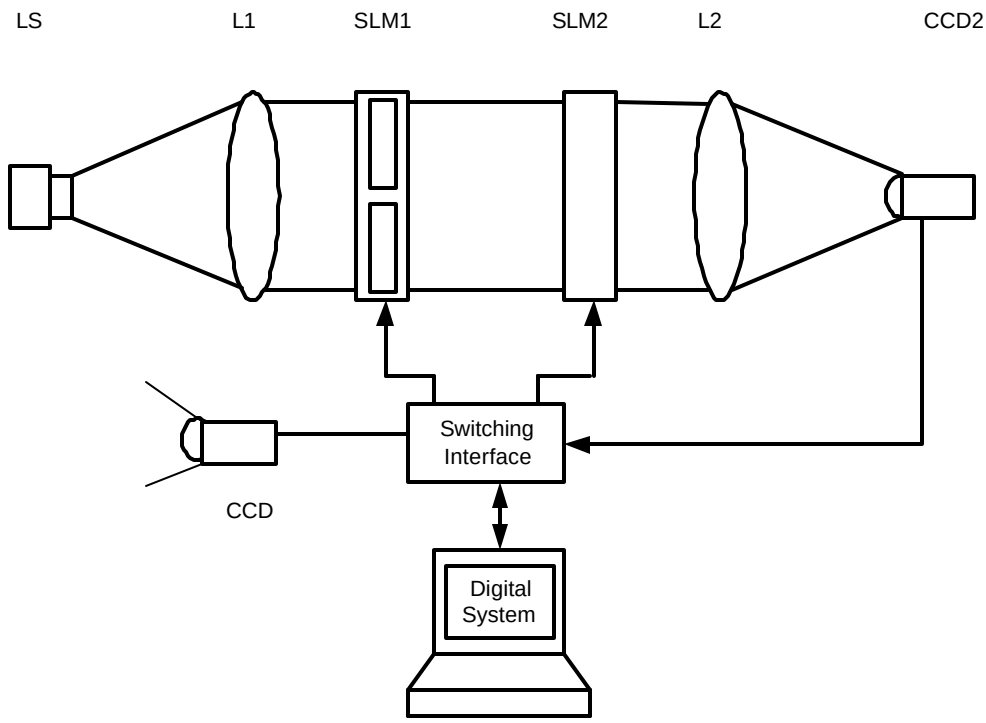

Figure 2-6: Fringe-Adjusted JTC

2.7 PHASE-ENCODED JTC

When the input scene consists of multiple images, the JPS is cluttered with correlation and autocorrelation peaks that distort each other and are hard to distinguish from one another. The Fourier plane image subtraction technique mentioned earlier is one of the method used eliminate the zero-order peak. The phase encoding technique is simpler method that can be employed to achieve the same effects without the need for digital computation and extra processing steps. The phase mask in this technique can be represented by [8, 27]

$$\Phi(u,v) = \exp[\, jy\,(u,v)] \tag{15}$$

where $y\,(u,v)$ is a random phase distribution between $-p$ and p .

$$f(x,y) = r(x, y+y_0) + \sum_{i=1}^{N} t_i(x, y-y_i) \otimes j_i(x,y) \tag{16}$$

where $j_i(x,y)$ is the spatial domain transformation of the phase mask. At the correlation output, the JPS captured is

$$\begin{aligned}
|F(u,v)|^2 &= \left| |T(u,v)| \exp[f_i(u,v)] \exp(juy_0) + \sum_{i=1}^{n} |R_i(u,v)| \exp[f_{ti}(u,v)] \exp(-juy_i) \times f(u,v) \right|^2 \\
&= |T(u,v)|^2 + \sum_{i=1}^{n} |R_i(u,v)|^2 \\
&+ \sum_{i=1}^{n} \{ |T(u,v)| |R_i(u,v)| \times \exp[f_t(u,v) - f_{ti}(u,v) + jv(y_0 + y_i)] \} \times \Phi_i^*(u,v) \\
&+ \sum_{i=1}^{n} \{ |T(u,v)| |R_i(u,v)| \exp[-f_t(u,v) + f_{ri}(u,v) - jv(y_0 + y_i)] \} \times \Phi_i(u,v) \\
&+ \sum_{i=1}^{n} \left\{ \sum_{k=1}^{i \neq k}{}^{n} \{ |R_i(u,v)| |R_k(u,v)| \times \exp[f_{ri}(u,v) - f_{rk}(u,v) - jv(y_i - y_k)] \} \times \Phi_k^*(u,v) \right\} \times \Phi_i(u,v) \\
&+ \sum_{i=1}^{n} \left\{ \sum_{k=1}^{i \neq k}{}^{n} \{ |R_i(u,v)| |R_k(u,v)| \times \exp[-f_{ri}(u,v) + f_{rk}(u,v) + jv(y_i - y_k)] \} \times \Phi_k(u,v) \right\} \times \Phi_i^*(u,v)
\end{aligned} \tag{17}$$

When JPS is multiplied by the same phase mask $\Phi(u,v)$, the cross correlation between the reference image and the test image is preserved while all other peaks are scattered in all directions and appear like noise (as shown in Figure 2-7).

$$
\begin{aligned}
F(u,v)^2 \times f_p(u,v) &= \left|T(u,v)\right|^2 \times f_p(u,v) + \sum_{i=1}^{n} \left|R_i(u,v)\right|^2 \times f_p(u,v) \\
&+ \left|T(u,v)\right|\left|R_p(u,v)\right| \times \exp\left[f_t(u,v) - f_{r_p}(u,v) \right] \\
&+ \sum_{i=1}^{n \neq p}^{n} \left\{ \left|T(u,v)\right|\left|R_i(u,v)\right| \times \exp\left[f_t(u,v) - f_{t_p}(u,v) + jv(y_0 + y_i) \right] \right\} \times \Phi_i^{*}(u,v) \times f_p(u,v) \\
&+ \sum_{i=1}^{n} \left\{ \left|T(u,v)\right|\left|R_i(u,v)\right| \times \exp\left[-f_t(u,v) + f_{ri}(u,v) - jv(y_0 + y_i) \right] \right\} \times \Phi_i(u,v) \times f_p(u,v) \\
&+ \sum_{i=1}^{n} \left\{ \sum_{k=1}^{i \neq k}^{n} \left\{ \left|R_i(u,v)\right|\left|R_k(u,v)\right| \times \exp\left[f_{ri}(u,v) - f_{rk}(u,v) - jv(y_i - y_k) \right] \right\} \times \Phi_k^{*}(u,v) \right\} \times \Phi_i(u,v) \times f_p(u,v) \\
&+ \sum_{i=1}^{n} \left\{ \sum_{k=1}^{i \neq k}^{n} \left\{ \left|R_i(u,v)\right|\left|R_k(u,v)\right| \times \exp\left[-f_{ri}(u,v) + f_{rk}(u,v) + jv(y_i - y_k) \right] \right\} \times \Phi_k(u,v) \right\} \times \Phi_i^{*}(u,v) \times f_p(u,v)
\end{aligned}
$$

(18)

Figure 2-7: Correlation output of a Phase Encoded JTC

To avoid affecting the overall speed of the phase encoded JTC, the phase masks are computed *a priori* and stored with the reference images in the digital system.

Figure 2-8 shows the architecture of a phase-encoded JTC, which is simple and cost effective to implement. The laser beam from source LS is split into two beams by beam splitter BS1 after being collimated by lens L1. At SLM1 the horizontal beam is modulated with input scene image captured by CCD1and loaded through the digital system switch to the upper part of the SLM3, which is a phase only SLM that is loaded via digital system with the spatial domain phase mask from the computer. The mirror M1 steers the Fourier transform of the phase encoded input scene performed by L2 into BS2. The vertical light from BS1 is steered by mirror M2 into SLM2, where it is modulated with the reference image that was loaded from the computer to the lower half of the SLM. BS2 combines the Fourier transform of the reference image performed by lens L3 and the Fourier transform of the phase-encoded input performed by L2. The Fourier domain version of the phase mask is downloaded to a phase only SLM4 such that the combined beam traveling through it is multiplied by the phase mask in Fourier domain. Lens L4 performs the inverse Fourier transform on the combined beam leaving SLM4. The power spectra is captured and recorded by CCD2 and then downloaded into the digital system.

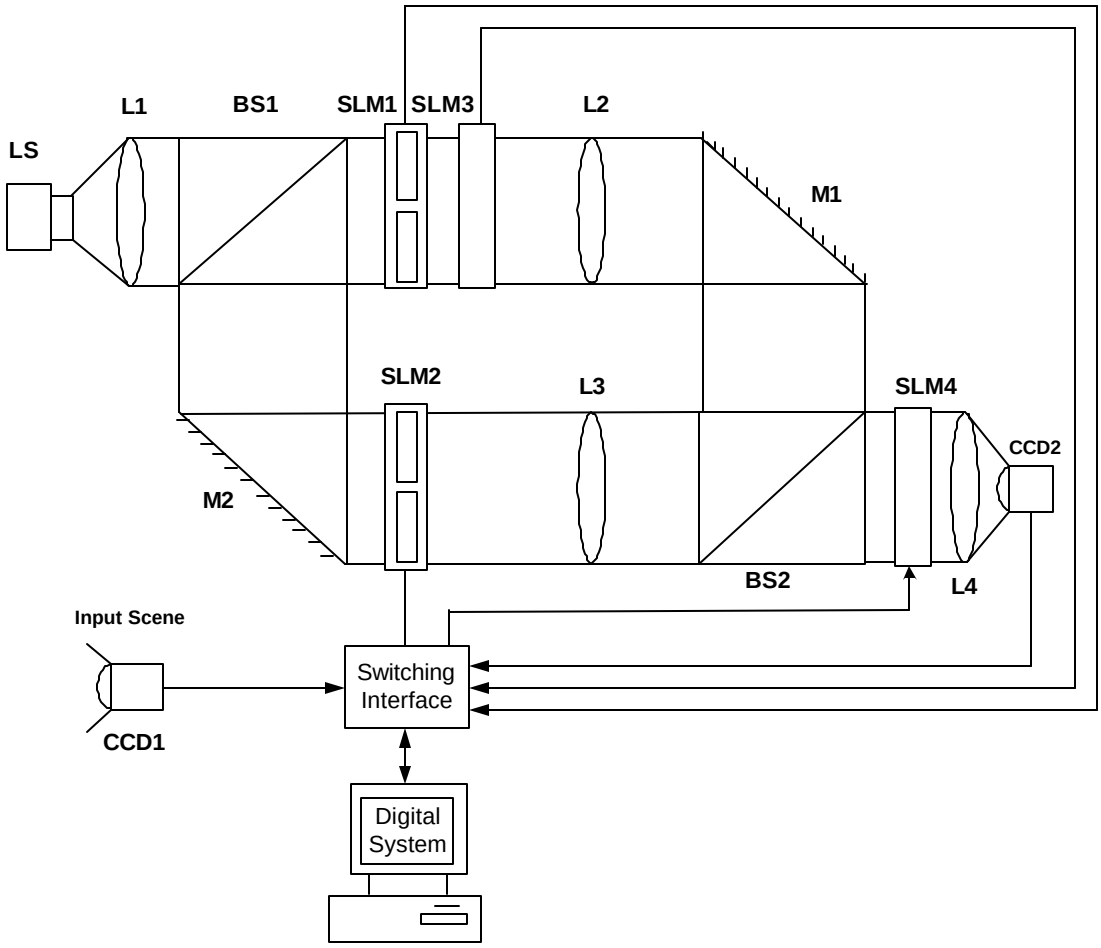

Figure 2-8: Phase Encoded JTC

3 RANDOM PHASE MASK

This section provides a short overview of the theory and application of Pseudo-random sequences, focusing mainly on how M-sequences are used to generate two dimensional array orthogonal phase masks. Pseudo-random sequences are defined as deterministic sequence of integers, which have been chosen in some methodical manner, but appear to be random [29].

3.1 M-SEQUENCE

In creating a phase mask, M-sequence is the preferred Pseudo-random sequence due to ease of generation. Maximal length sequences (M-sequences) have been utilized widely in numerous modern communications since first introduced by Zierler in 1967 [30] and their theoretical foundations were greatly expanded by Golomb [31]. For randomness, the following properties must be satisfied [32]:

- Balance: – the number of ones (high state) in one period must be equal to the number of zeros (low state), or the difference of the number of ones $(x^n - 1)$ and zeros $(x^{n-1} - 1)$ should not be more than one.
- Run Property: – defined as a maximal string of consecutive identical symbols (zeros or ones) in the sequence. For M-sequence in a period, half of the runs have a length 1, one quarter have length 2, one eighth of length 3.
- Shift Property: – an M-sequence $\{S_k\}$ when shifted cyclically (modulo the sequence length) is still an M-sequence.

A linear feedback shift register with a generating polynomial $g(x)$ in which a coefficient arises from the Galois field [32] can be used generate M-sequence. Finite (Galois) fields are fields with only a finite number of elements that are closed under operations of addition, subtraction, multiplication, and division by non-zero elements. These fields exist only when the elements are p^N where P is a prime and N any positive integer.

Figure 3-1 is simple set up of shift registers whose contents modified at every step by a binary – weighted value of the output stage. Considering the initial state of the registers and the feedback arrangement, the LSFR method generates a sequence {b} that satisfies linear recursion formula.

$$S_{i+n} = b_{n-1}S_{i+n-1} + ... + b_0 S_i \qquad (19)$$

where feedback coefficients are $b_{n-1}, b_n, ...b_1, b_0 \in F=\{0,1\}$

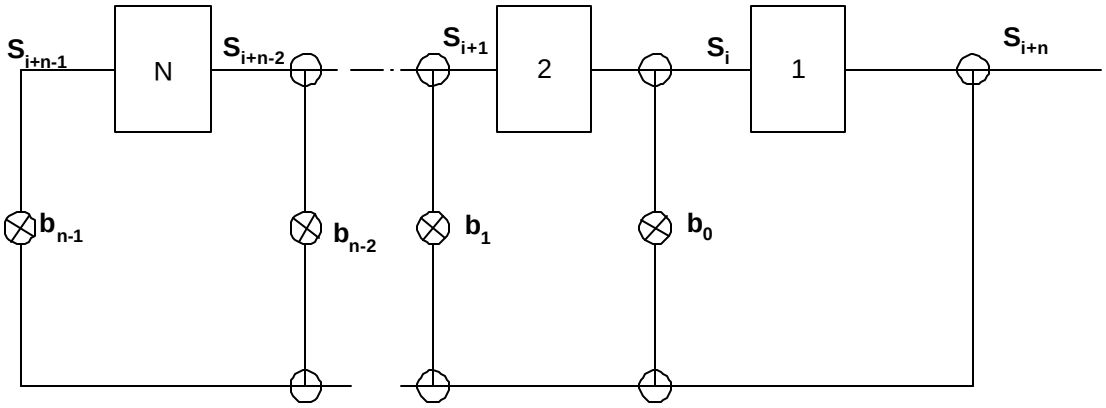

Figure 3-1: Generalized Generator

The succession state of the LFSR form a purely period sequence of period length $d \le 2^k - 1$ where k is the order of the shift register sequence. To derive the characteristic polynomial of shift register sequences we use the generating function defined as

$$G(x) = \sum_{i=0}^{\infty} b_i x^i \tag{20}$$

where x is an indeterminate

$G(x)$ reflects the properties of the sequence {b} and represent its terms in correct order

$$\begin{aligned} G(x) &= \sum_{i=0}^{\infty} \sum_{j=0}^{k} a_j b_{i-j} x^i \\ &= \sum_{j=0}^{k} a_j x^j \sum_{i=0}^{\infty} b_{i-j} x^{i-j} \\ &= \sum_{j=0}^{k} a_j x^j \left(b_{-j} x^{-j} + \ldots + b_{-1} x^{-1} + \sum_{i=0}^{\infty} b_i x^i \right) \end{aligned} \tag{21}$$

Thus

$$G(x) = \sum_{j=1}^{k} a_j x^j \left(b_{-j} x^{-j} + \ldots + b_{-1} x^{-1} + G(x) \right) \qquad \text{and}$$

$$G(x) = \frac{\sum_{j=1}^{k} a_j x^j \left(b_{-j} x^{-j} + \ldots + b_{-1} x^{-1} \right)}{1 - \sum_{j=1}^{k} a_j x^j} \tag{22}$$

In equation (21) $G(x)$ can be separated into $\left(b_{-j} x^{-j} + \ldots + b_{-1} x^{-1} \right)$ which are terms for initial state and feedback coefficient $\sum_{j=1}^{k} a_j$. The denominator $1 - \sum_{j=1}^{k} a_j x^j$ is independent of the initial state thus for b (values of 0 and 1 equation (21) can be expressed as

$$G(x) = \frac{a_k}{1 - \sum_{j=1}^{k} a_j x^j} \tag{23}$$

If you let

$$\begin{aligned} f(x) &= 1 - \sum_{j=1}^{k} a_j x^j \\ &= 1 - a_1 x - a_2 x^2 - \ldots - a_{k-1} x^{k-1} - a_k x^k \\ &\equiv 1 + a_1 x + a_2 x^2 + \ldots + a_{k-1} x^{k-1} + a_k x^k \,(\mathrm{mod} 2). \end{aligned} \tag{24}$$

If we assume a_k is non-zero (i.e. $a_k = 1$) and the characteristic polynomial $f(x)$ is expressed in k^{th} degree to be

$$f(x) = x^k + a_{k-1} x^{k-1} + \ldots + a_1 x + 1 \tag{25}$$

For a given initial state

$$G(x)=\frac{1}{f(x)}=\sum_{i=0}^{\infty}b_i x^i \tag{26}$$

As earlier stated sequence {b} generated from LSFR is periodic at length $d \le 2^k - 1$

Suppose the sequence {b} have a period length of d

$$\begin{aligned}\frac{1}{f(x)} &= (b_0 + b_1 x + \ . \ . \ . \ + b_{d-1}x^{d-1}) + x^d(b_0 + b_1 x + \ . \ . \ . \ + b_{d-1}x^{d-1}) \\ &\quad + x^{2d}(b_0 + b_1 x + \ . \ . \ . \ + b_{d-1}x^{d-1}) + \ . \ . \ . \\ &= (b_0 + b_1 x + \ . \ . \ . \ + b_{d-1}x^{d-1})(1 + x^d + x^{2d} + x^{3d} + \ . \ . \ .) \\ &= (b_0 + b_1 x + \ . \ . \ . \ + b_{d-1}x^{d-1}) \Big/ (1 - x^d).\end{aligned} \tag{27}$$

Since $f(x)$ is characteristic polynomial it divides by $1 - x^d$ and the quotient can be expressed as

$$b_0 + b_1 x + \ . \ . \ . \ + b_{d-1}x^{d-1} \tag{28}$$

then

$$\begin{aligned}\frac{1}{f(x)} &= \frac{b_0 + b_1 x + \ . \ . \ . \ + b_{d-1}x^{d-1}}{1 - x^d} \\ &= (b_0 + b_1 x + \ . \ . \ . \ + b_{d-1}x^{d-1})(1 + x^d + x^{2d} + \ . \ . \ . \ ) \\ &= (b_0 + b_1 x + \ . \ . \ . \ + b_{d-1}x^{d-1}) + x^d(b_0 + b_1 x + \ . \ . \ . \ + b_{d-1}x^{d-1}) + \ . \ . \ . \\ &= G(x) = \sum_{i=0}^{\infty} b_i x^i\end{aligned} \tag{29}$$

This shows that for a sequence {b} with a period length d, the equating coefficients are similar to the powers of x.

$$\{b_i\} = \{b_i\} \tag{30}$$

Table 3.1 contain M-sequence feedback sets for LFSR [33].

Shift Register length, n	Possible Feedback Taps
2	[2,1]
3	[3,1]
4	[4,1]
5	[5,2], [5,4,3,2], [5,4,2,1]
6	[6,1], [6,5,2,1], [6,5,3,2]
7	[7,1], [7,3], [7,3,2,1], [7,4,3,2], [7,6,4,2], [7,6,3,1],[7,6,5,2], [7,6,5,4,2,1], [7,5,4,3,2,1]
8	[8,4,3,2], [8,6,5,3], [8,6,5,2], [8,5,3,1], [8,6,5,1],[8,7,6,1], [8,7,6,5, 2,1], [8,6,4,3,2,1]

Table 3-1: Polynomial Roots

3.2 TWO DIMENSIONAL ARRAYS

Two-dimensional arrays can be implemented using the following methods.

- Folding Array: - Mac Williams and Sloane [34] and Green [35] used this method to create a matrix of the same periodic autocorrelation as the M-sequence. To implement a 2D array, a sequence of length pq is remapped into array of area pq with p and q being co-primes.
- Distinct Sum Arrays: - In this method, an array is generated by placing a suitable sequence in the top row and applying differential cyclic shifts to generate the rows after. The construction method is

based on the concept that all accumulated cyclic shifts between rows separated by distance d are different (Distinct sums property) [35].

- Product array: – a 2D array is created by multiplying two sequences r and s of lengths p and q element by element. If the two sequences r and s are equal $(r = s)$ then operation can be reduced to a shift-and-add operation. In 1991, Kuo and Rigasi [36] used this method to create m-arrays, which have found applications in coded aperture imaging, pattern synchronization, code division and image multiplexing.

3.2.1 Shift and add property

When an M-sequence is shifted in time and added (modulo 2) to a non-shifted version of the same sequence, an identical sequence shifted by certain number of bits is the result as shown in Figure 3-2.

$$u^i + u^j = u^k \tag{31}$$

For $0 < i, j, k < 2^n - 1$ and u^k is the shifted M-sequence (by k positions) while u is the original M-sequence.

For example:

$$\begin{array}{rll} & u & 111100010011010 \\ \oplus & u^4 & 101011110001001 \\ \hline & u^3 & 010111100010011 \end{array}$$

$\oplus$ represents bit by bit modulo two addition.

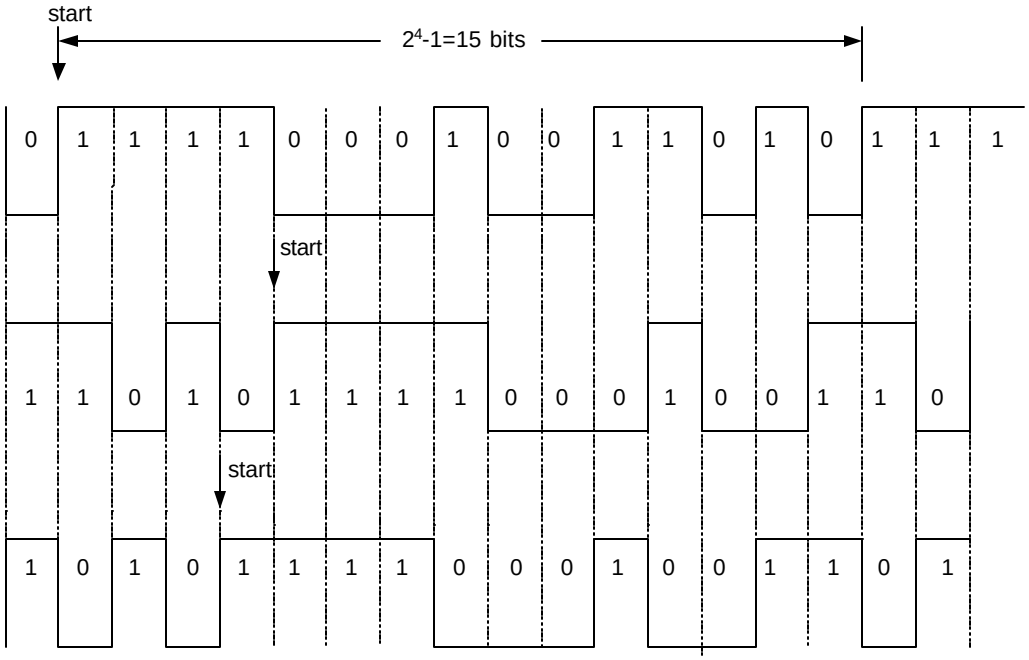

Figure 3-2: Addition of Two Sequences

A shift i to the left is equivalent of $(2^n - 1 - i)$ position shifted to the left, thus the following equation

$$u^i = u^{i \pm (2^n - 1)} \qquad (32)$$

for $0 \le i < 2^n - 1$

Using the above theory a two dimensional m-array can be constructed from two M-sequence [a] and [b].where $[a] = [a_0, a_1 ....., a_{n_a - 1}]$ and $[b] = [b_0, b_1 ....., b_{n_b - 1}]$ to form [M] as in equation (33)

$$[M] = \begin{bmatrix} a_0 \otimes b_0 & a_0 \otimes b_1 & . \; . \; . & a_0 \otimes b_{n_b - 1} \\ a_1 \otimes b_0 & a_1 \otimes b_1 & . \; . \; . & a_1 \otimes b_{n_b - 1} \\ . & . & . \; . \; . & . \\ . & . & . \; . \; . & . \\ . & . & . \; . \; . & . \\ a_{n_a - 1} \otimes b_0 & a_{n_a - 1} \otimes b_1 & . \; . \; . & a_{n_a - 1} \otimes b_{n_b - 1} \end{bmatrix} \qquad (33)$$

Since every row and column is a modulo-2 addition of an M-sequence, the m-array consists of M-sequences and their complement, thus preserving all their properties as shown in Figure 3-3. In addition, there is more freedom in selecting the size of the array.

For example:

$$
\begin{array}{cll}
 & u & 111100010011010 \\
\oplus & u^4 & 101011110001001 \\
\hline
 & u^3 & 010111100010011
\end{array}
$$

⊕	1	0	1	0	1	1	1	1	0	0	0	1	0	0	1
1	0	1	0	1	0	0	0	0	1	1	1	0	1	1	0
1	0	1	0	1	0	0	0	0	1	1	1	0	1	1	0
1	0	1	0	1	0	0	0	0	1	1	1	0	1	1	0
1	0	1	0	1	0	0	0	0	1	1	1	0	1	1	0
0	1	0	1	0	1	1	1	1	0	0	0	1	0	0	1
0	1	0	1	0	1	1	1	1	0	0	0	1	0	0	1
0	1	0	1	0	1	1	1	1	0	0	0	1	0	0	1
1	0	1	0	1	0	0	0	0	1	1	1	0	1	1	0
0	1	0	1	0	1	1	1	1	0	0	0	1	0	0	1
0	1	0	1	0	1	1	1	1	0	0	0	1	0	0	1
1	0	1	0	1	0	0	0	0	1	1	1	0	1	1	0
1	0	1	0	1	0	0	0	0	1	1	1	0	1	1	0
0	1	0	1	0	1	1	1	1	0	0	0	1	0	0	1
1	0	1	0	1	0	0	0	0	1	1	1	0	1	1	0
0	1	0	1	0	1	1	1	1	0	0	0	1	0	0	1

Figure 3-3: Example of m-array

3.2.2 Array Auto-Correlation

The cyclic auto correlation $\Theta_{AA(i,j)}$ of two-dimensional m-array is expressed as

$$\begin{cases} \Theta_{AA(i,j)} = & 1, & for & i \neq 0 \,\&\, j \neq 0 \\ \Theta_{AA(i0)} = & -n_b, & for & i \neq 0 \\ \Theta_{AA(0,j)} = & -n_a, & for & i \neq 0 \\ \Theta_{AA(0,0)} = & n_a n_b, & for & i \neq 0 \end{cases} \tag{34}$$

By definition, it measures how an array matches a copy of itself as the copy is shifted and mathematical proven in [36].

3.2.3 Array Cross-Correlation

The cyclic cross correlation $\Theta_{AA'(i,j)}$ between two different two-dimensional m-arrays $[A]$ and $[A']$ can be expressed as

$$\Theta_{AA'(i,j)} = \Theta_{aa'(i)}\Theta_{bb'(j)} \tag{35}$$

where $[A']$ is a m-array generated by $[a']$ and $[b']$ [37] and measures how the interference between the two different arrays.

3.3 RANDOM PHASE MASK ALGORITHM

In this section, we describe a step-by-step procedure to design an optical phase mask. The steps involves designing an M-sequence from a LFSR and using it to generate a two dimensional orthogonal array which is converted to phase mask. These steps are summarized in Figure 3-4.

Input: A sequence $a^i \equiv (a_0^i, a_1^i, ...a_{N-1}^i)$

Output: Random Phase Mask

1. Generate M-sequence $a^i \equiv (a_0^i, a_1^i, ...a_{N-1}^i)$

   where $i = 0$ for original sequence.

2. Generate shifted sequences $a^i \equiv (a_0^i, a_1^i, ...a_{N-1}^i)$

   where $i = 1,2,.....N-1$ for N is the length of the sequence code.

3. For $0 \le i \le N-1$ choose two sequence codes A and B ($A \neq B$) from

   $a^i \equiv (a_0^i, a_1^i, ...a_{N-1}^i)$ and create a two vectors [A] and [B^T]

   where T represents transpose.

4. Using modulo 2 additions, add bit by bit the two vectors to form a matrix M.

5. create a matrix consisting of $(N+1)\times(N+1)$ zeros and add two the matrix M to form a padded M matrix.

6. For $M = (m_{i,j})$ where $i = j = N+1$ Convert 1 and 0 to respective phase angles (1 for p and 0 for 0).

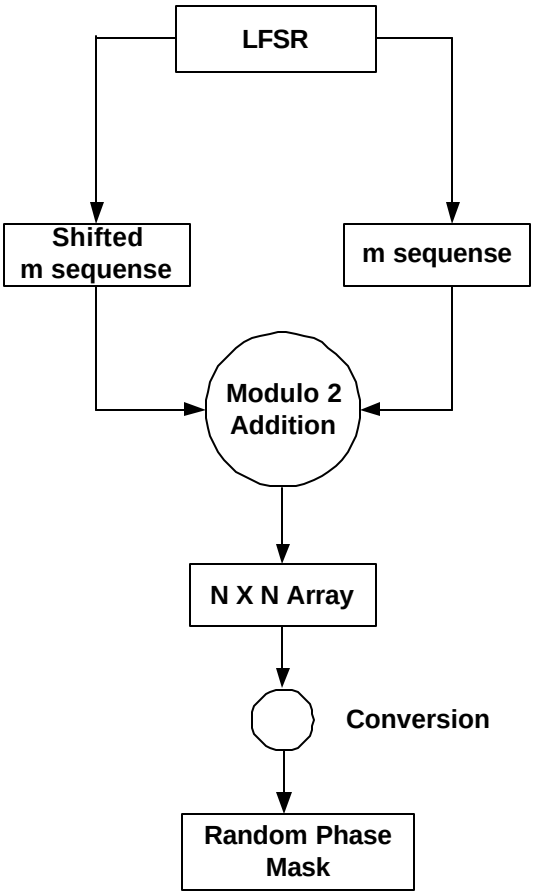

Figure 3-4: Formulation of Random Phase Mask

3.4 COMPARISON OF DIFFERENT ENCODING LEVELS

Histograms have been widely used to represent, analyze, and characterize images. They are easy to compute and represent the approximations of the probability density functions of random variables whose realization is the particular set of pixel values found in the images. In order to investigate the effects of varying levels of phase encoding of the phase masks implemented with maximal length sequence, we first analyze the histograms of images phase encoded with different levels: binary (2), ternary (3)and five level (5). General length (n) of a

M-sequence is represented by equation $n = m^x - 1$, where m (m = 2, 3, 5) is the level of encoding selected. From the figures below (Figure 3-5, Figure 3-6, Figure 3-7), several observations can be made about the distribution of the phases in the encoded image. As we increase the number of levels (m), the peak height of the histograms increase and the curve smoothens. Figure 3-7 (m=5) offers best results compared to the other two encoding levels (m= 2, 3).This implies that when the reference image is encoded into more phase mask thus more pixels, it offers better results. In addition, we note that when identical images are multiplied with different randomized phase masks, their histograms plots are of Gaussian shape but of different heights.

Figure 3-5: Histogram of binary encoding (m=2)

Figure 3-6: Histogram of ternary encoding (m=3)

Figure 3-7: Histogram of level five encoding (m=5)

Next, we consider the influence of the phase encoding levels on the performance of the phase encoded JTC. Using the selected three levels (m = 2, 3, 5) to create different phase masks, the following correlation outputs were observed at the output plane of JTC system. Figure 3-8 shows the

correlation output of the phase encoded JTC binary encoded phase mask. The presence of two peaks at the correlation output deviates from the expected results. The presence of a conjugate cross correlation peak in the output plane confirms the inability of binary two phase to disperse all undesired peaks. From this, we can infer that a phase mask created from a binary M-sequence is not suitable for encoding images in the JTC system.

Through comparison, level- 5 encoding represented by correlation output in Figure 3-10 has a better correlation output compared to binary and ternary encoding. The correlation peaks are distinguished clearly and their intensity height increases as the number of levels were increased (from 2, 3, and infinity for rand sequence). Figure 3-11 shows the correlation output when phase mask is created from a random sequences (Matlab rand function was used to create the Pseudo random sequence).

Figure 3-8: Correlation Outputs for Image created with a Random phase mask (m=2)

Figure 3-9: Correlation Outputs for Image created with a Random phase mask (m=3)

Figure 3-10: Correlation Outputs for Image created with a Random phase mask (m=5)

Figure 3-11: Correlation Outputs for Image created with a Random phase mask

4 MULTI-REFERENCE PHASE ENDODED JTC

This section presents an analysis of the multi-reference phase encoded JTC and sheds light on the implemented multi-reference phase encoded JTC using a phase only SLM. The goal of the section is to mathematical express the mentioned architectures and compares their results.

Using a multiple reference image in the input joint image to correlate with a single test image in a single step, Alsamman [37] presented a multiple reference phase encoded JTC that takes advantage of the massive parallelism of optical systems to increase the processing power of the JTC. In this technique, reference images are phase encoded using Pseudo-random sequences, hence removing extraneous peaks from correlation plane as well as improving the spatially efficiency of the JTC system.

In a classical JTC, a minimum SLM size of 2N X 2N is required to correlate two N X N images. This is because of the displacement $(2y_0)$ required between the reference image and the test image to avoid zero order term in the correlation output dominating and overshadowing the cross correlation terms. A displacement of distance $(2y_0)$ at the input plane results in double distance ($4y_0$ between the cross correlation terms) at output plane. In order to obtain large displacement without increasing the sizes of the SLM, small images are used which result to a lower discrimination power at correlation output plane. The use of large SLM size vastly increases the overall cost of the JTC while increasing the overall system size.

In the multi-reference phase encoding technique, every reference image is multiplied with a phase mask defined as

$$\Phi(u,v) = \exp[\, jy\,(u,v)] \tag{36}$$

where $y(u,v)$ is a random phase distribution between $-p$ and p.

The joint input image of multi-reference phase encoded JTC represented by the equation below consists of a reference image $r_i(x,y)$ that has been encoded with phase mask $j_i(x,y)$ and displayed side by side with an input test image.

$$f(x,y) = t(x,y) + \sum_{i=1}^{N} r_i(x,y) \otimes j_i(x,y) \tag{37}$$

Using light from source LS and collimated by lens L1, the joint input image is displayed on SLM1 (Figure 4-1). The converging lens L2 is used to obtain the Fourier transform of joint input image and the JPS captured by the CCD device and routed to SLM1 through the digital interface as shown on Figure 4-1

$$\begin{aligned}
F(u,v)^2 &= \left| |T(u,v)| \exp[f_i(u,v)] + \sum_{i=1}^{n} |R_i(u,v)| \exp[f_{ti}(u,v)] \times f(u,v) \right|^2 \\
&= |T(u,v)|^2 + \sum_{i=1}^{n} |R_i(u,v)|^2 \\
&+ \sum_{i=1}^{n} \{ |T(u,v)| |R_i(u,v)| \times \exp[f_t(u,v) - f_{ti}(u,v)] \} \times \Phi_i^*(u,v) \\
&+ \sum_{i=1}^{n} \{ |T(u,v)| |R_i(u,v)| \exp[-f_t(u,v) + f_{ri}(u,v)] \} \times \Phi_i(u,v) \\
&+ \sum_{i=1}^{n} \left\{ \sum_{k=1}^{i \neq k}{}^{n} \{ |R_i(u,v)| |R_k(u,v)| \times \exp[f_{ri}(u,v) - f_{rk}(u,v)] \} \times \Phi_k^*(u,v) \right\} \times \Phi_i(u,v) \\
&+ \sum_{i=1}^{n} \left\{ \sum_{k=1}^{i \neq k}{}^{n} \{ |R_i(u,v)| |R_k(u,v)| \times \exp[-f_{ri}(u,v) + f_{rk}(u,v)] \} \times \Phi_k(u,v) \right\} \times \Phi_i^*(u,v)
\end{aligned} \tag{38}$$

To obtain results for a particular reference image, its corresponding phase mask is displayed on SLM2 and correlated through lens L2. The same process can be achieved by multiplying the JPS digitally with the phase mask

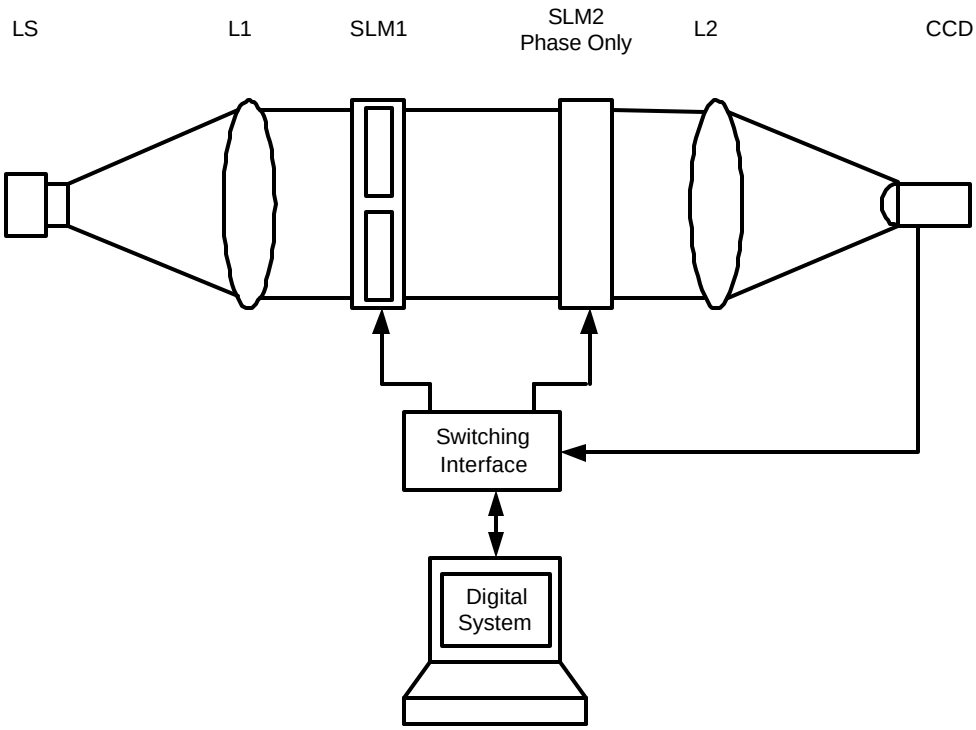

Figure 4-1: Multi-Reference Phase Encoded JTC

Figure 4-2 shows the joint input image with two reference image of size 256 X 256 pixels phase encoded with a phase mask created from five level maximal length sequences (M-sequences). The shift and add method described in chapter three was used to create an m-array which was translated into a phase mask of size 256 X 256. In Figure 4-2 below only the test image can clearly be identified, as the phase encoded reference images pixels are scattered by the phase mask in all directions and appear as noise. Figure 4-3 represents the correlation output achieved using a multi-referenced phase encoded JTC.

Figure 4-2: Joint Input Image

Figure 4-3: Output of JTC

4.1 MULTI-REFERENCE PHASE ENCODED JTC USING PHASE SLM ONLY

In this thesis, we further improve the performance of the multi-reference phase encoded JTC by converting both the reference and target image into phase information before applying operations similar to multi-reference phase encoded JTC discussed earlier. From the previous phase encoding technique, we have seen that Fourier plane image subtraction technique results are attained using a random phase mask generated from two-dimensional M-sequence array. The advantage of this method is that the same effects are achieved with less digital computation and without extra processing steps [37]. Phase encoding technique has also been successful used in the field of information security as in optical authenticity verification [38] and in storing encrypted information holographical [39].

In the initial stage, all images are encoded with a phase expression forming a phase only representation. Target image and reference image are converted into the following expressions

$$pt(x,y) = \exp[\, jA\{t(x,y)\}] \tag{39}$$

$$pr(p,q) = \exp[\, jA\{r(x,y)\}] \tag{40}$$

where A is phase depth $(2p)$

The technique of transforming intensity images into phase function has been previous used in pattern recognition pattern [38,39]. The joint input image used in this system consists of target image placed side by with multiplexed references images as expressed below equation and shown in Figure 4-4:

$$pf(x,y) = pt(x,y) + \sum_{i=1}^{N} pr_i(x,y) \otimes j_i(x,y) \tag{41}$$

where $j_i(x,y)$ is the spatial domain transformation of the phase mask that is expressed as

$$\Phi(u,v) = \exp[\, jy\,(u,v)] \tag{36}$$

where $y\,(u,v)$ is a phase distribution between $-p$ and p created using an M-sequence

Different shifts of M-sequence are used to create orthogonal phase masks that are used multiplied with every reference image in Fourier domain.

Figure 4-4: Joint Input Image

The JPS collected by CCD at the correlation output can be expressed as

$$
\begin{aligned}
\left|PF(u,v)\right|^2 &= \left|\left|PT(u,v)\right|\exp\left[f_i(u,v)\right]+\sum_{i=1}^{n}\left|PR_i(u,v)\right|\exp\left[f_{ti}(u,v)\right]\times f(u,v)\right|^2 \\
&= \left|PT(u,v)\right|^2+\sum_{i=1}^{n}\left|PR_i(u,v)\right|^2 \\
&+\sum_{i=1}^{n}\left\{\left|PT(u,v)\right|\left|PR_i(u,v)\right|\times\exp\left[f_t(u,v)-f_{ti}(u,v)\right]\right\}\times\Phi_i^{*}(u,v) \\
&+\sum_{i=1}^{n}\left\{\left|PT(u,v)\right|\left|PR_i(u,v)\right|\exp\left[-f_t(u,v)+f_{ri}(u,v)\right]\right\}\times\Phi_i(u,v) \\
&+\sum_{i=1}^{n}\left\{\sum_{k=1}^{i\neq k}^{n}\left\{\left|PR_i(u,v)\right|\left|PR_k(u,v)\right|\times\exp\left[f_{ri}(u,v)-f_{rk}(u,v)\right]\right\}\times\Phi_k^{*}(u,v)\right\}\times\Phi_i(u,v) \\
&+\sum_{i=1}^{n}\left\{\sum_{k=1}^{i\neq k}^{n}\left\{\left|PR_i(u,v)\right|\left|PR_k(u,v)\right|\times\exp\left[-f_{ri}(u,v)+f_{rk}(u,v)\right]\right\}\times\Phi_k(u,v)\right\}\times\Phi_i^{*}(u,v) \qquad (42)
\end{aligned}
$$

By multiply the JPS with conjugate phase mask, we get the following expression

$$
\begin{aligned}
\left|PF(u,v)\right|^2 \times \Phi_p(u,v) &= \left|\left|PT(u,v)\right|\exp\left[f_i(u,v)\right] + \sum_{i=1}^{n}\left|PR_i(u,v)\right|\exp\left[f_{ti}(u,v)\right]\times f(u,v)\right|^2 \times \Phi_p(u,v) \\
&= \left|PT(u,v)\right|^2 \times \Phi_p(u,v) + \sum_{i=1}^{n}\left|PR_i(u,v)\right|^2 \times \Phi_p(u,v) \\
&+ \sum_{\substack{i=1 \\ n\neq p}}^{n}\left\{\left|PT(u,v)\right|\left|PR_i(u,v)\right|\times\exp\left[f_t(u,v) - f_{tp}(u,v)\right]\right\}\times\Phi_i^*(u,v)\times\Phi_p(u,v) \\
&+ \sum_{i=1}^{n}\left\{\left|PT(u,v)\right|\left|PR_i(u,v)\right|\exp\left[-f_t(u,v) + f_{ri}(u,v)\right]\right\}\times\Phi_i(u,v)\times\Phi_p(u,v) \\
&+ \sum_{i=1}^{n}\left\{\sum_{\substack{k=1 \\ i\neq k}}^{n}\left\{\left|PR_i(u,v)\right|\left|PR_k(u,v)\right|\times\exp\left[f_{ri}(u,v) - f_{rk}(u,v)\right]\right\}\times\Phi_k^*(u,v)\right\}\times\Phi_i(u,v)\times\Phi_p(u,v) \\
&+ \sum_{i=1}^{n}\left\{\sum_{\substack{k=1 \\ i\neq k}}^{n}\left\{\left|PR_i(u,v)\right|\left|PR_k(u,v)\right|\times\exp\left[-f_{ri}(u,v) + f_{rk}(u,v)\right]\right\}\times\Phi_k(u,v)\right\}\times\Phi_i^*(u,v)\times\Phi_p(u,v)
\end{aligned}
\tag{43}
$$

The final correlation output is represented by Figure 4-5 below:

Figure 4-5: Correlation Output of Modified JTC

$$O(u,v)=\left[\left|PT(u,v)\right|^2+\sum_{i=1}^{n}\left|PR_i(u,v)\right|^2\right]\times\Phi(u,v)$$
$$+\sum_{i=1}^{n}\left|PT(u,v)\right|\left|PR_i(u,v)\right|\times\exp\left[f_r(u,v)-f_{ti}(u,v)+ju(y_0+y_i)\right]$$
$$+\sum_{i=1}^{n}\left|PT(u,v)\right|\left|PR_i(u,v)\right|\times\exp\left[-f_r(u,v)+f_{ti}(u,v)-u(y_0-y_i)\right]\times\Phi(u,v)\times\Phi(u,v)$$
$$+\sum_{i=1}^{n}\sum_{\substack{k=1\\ i\neq k}}^{n}\left|PR_i(u,v)\right|\left|PR_k(u,v)\right|\times\cos\left[f_{ti}(u,v)-f_{tk}(u,v)-u(y_i-y_k)\right]\times\Phi(u,v) \quad (45)$$

The random phase mask scatters all terms except the desired cross-correlation between the test image and the various reference images (see the second term in the above equation).

A reduced efficient architecture for the opto-electronic implementation of the multi- referenced JTC is shown in Figure 4-6. In this setup, Lens I is used to collimate a light from a light source LS, while Lens 2 performs the Fourier transform of the input joint image and a CCD camera is used to capture the corresponding joint power spectrum (JPS) . The joint input image consisting of phase encoded reference images and the test image are displayed using SLM1, which is a phase only SLM where the phase part of the images are presented. The Fourier transform of the joint input is performed by L2 while the JPS is captured by CCD2 downloaded to the digital system before being loaded back to the SLM1.

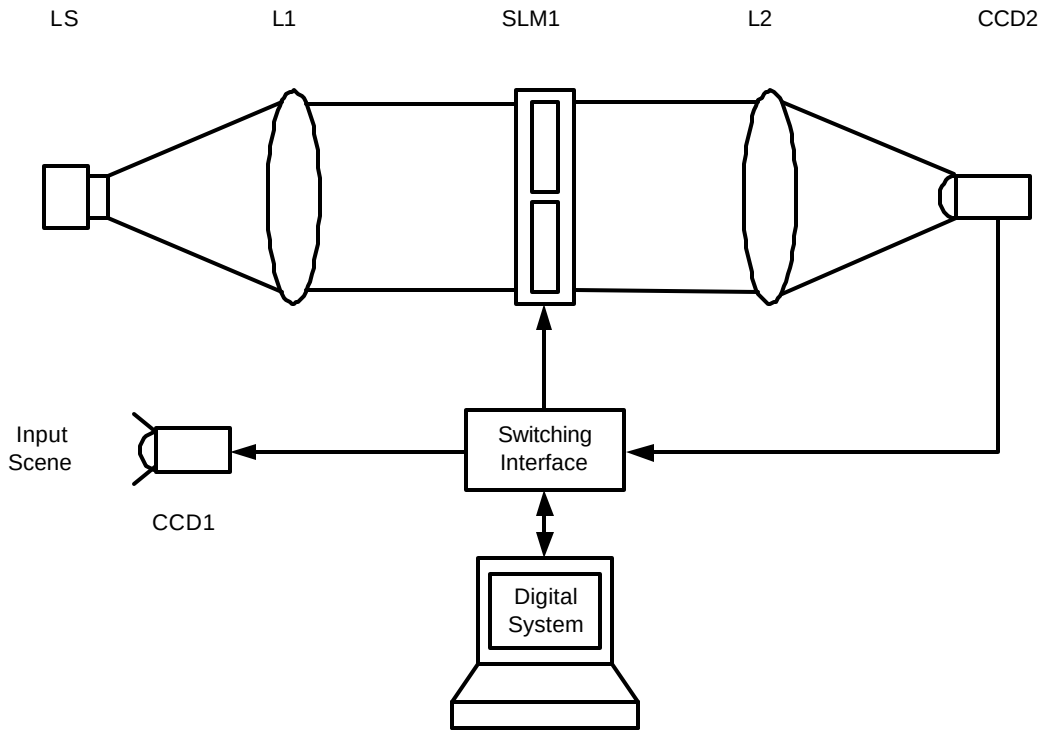

Figure 4-6: Multi-reference Phase Encoded JTC Using Phase SLM Only

Since the joint input images information is in phase only, The JTC architecture requires one SLM compared to two used in the previous techniques (Figure 4-1). As mentioned earlier the reduction of SLM sizes and number of SLMs used reduces the overall cost of the JTC system tremendously and improves simplicity, compactness and the feasibility for effective optical implementation.

4.2 COMPARISON OF CORRELATION OUTPUT RESULTS

In order to properly quantify the performance of the implemented system, a comparison was made with a multi-reference phase encoded JTC system using an identical simulation environment (identical image and same SLM size). All simulations were performed with mathematical software Matlab and correlation output of each reference image displayed on the same page for easy comparison

(see Figure 4-8 and Figure 4-9). For simulation, two reference images were phase masked and placed side by side to the input test image to form a joint input image as shown in Figure 4-7 but the images multiplied with phase mask appear as noise as shown in Figure 4-4

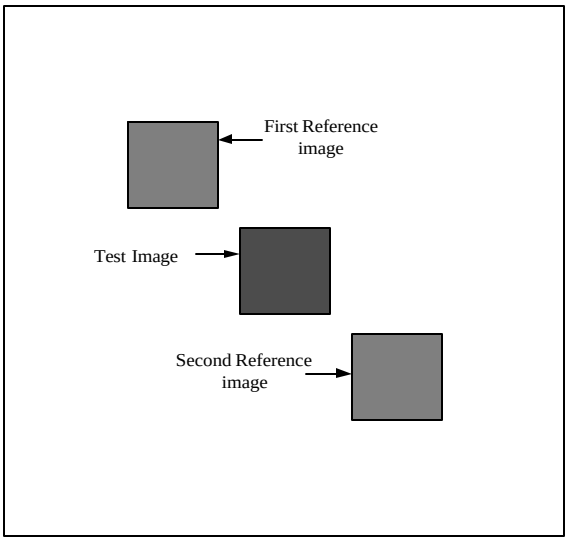

Figure 4-7: Joint Input Image Correlation Outputs

Figure 4-8 (a) and (b) illustrates the correlation output between the first reference image and the test image for the original multi-reference phase encoded JTC [38] and multi-reference phase encoded JTC using phase only SLM respectively.

As suggested in the previous section, comparing the correlation output between the two architectures we notice that the height of correlation peak increased and width of peak decreased with the use of phase information for correlation as described in section 4.2.

Figure 4-9 (a) and (b) displays the second correlation output between the second reference image and the test image for the ordinary multi-reference phase encoded JTC and the modified multi-reference phase encoded JTC which uses phase only SLM respectively.

(a)

(b)

Figure 4-8: First Reference Image Correlation Outputs

Correlation output from the multi-reference phase encoded JTC that uses phase only SLM represented by Figure 4-8 (b) and Figure 4-9 (b) clearly a vast improvement when compared to the correlation output from the previous method.

(a)

(b)

Figure 4-9: Second Reference Image Correlation Outputs

4.3 PERFORMANCE EVALUATION

To evaluate the effectiveness of the implemented system, we will look at performance metrics, which are based on the output plane correlation. Although the performance of most correlators depend on the type of images, random phase used and noise present in the input scene, our evaluation and simulation are based on the sizes of both the images and SLMs. In all our simulations an image of a rose flower (Figure 4-10) was used

Figure 4-10: Image of a Rose Flower

- Peak to Side Lobe Ratio (PSR)

Peak to side lobe ratio (PSR) defined below is used to measure the peak sharpness.

$$PSR = \frac{I_{cpi} - m}{s} \tag{46}$$

where m and s represents mean value and standard deviation of the correlation output excluding the peak location. While I_{cpi} is correlation peak intensity.

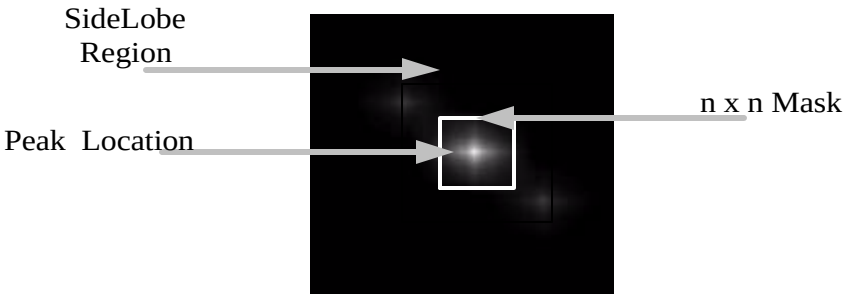

Figure 4-11: Peak to Side lobe ratio estimation

To estimate the PSR defined above, first the maximum correlation peak is located as indicated by a bright pixel in the center of the figure and its coordinates obtained using the following equation

$$(\hat{x},\hat{y}) \in \max(I_{mn}) \tag{47}$$

where $(\hat{x},\hat{y})$ are the coordinates of the maximum peak and I_{mn} are correlation coefficients.

To compute the mean m and the standard deviation of output a *n* X *n* Zero mask is created around the peak.

$$m = \frac{1}{MN}\sum_{1}^{N}\sum_{1}^{M} I(m,n) \tag{48}$$

- Peak to Correlation Energy (PCE)

PCE is the ratio of the correlation peak intensity to the correlation plane energy expressed as

$$PCE = \frac{I_{cpi}}{\sum_{y}\sum_{x}\left|c(x,y)\right|^2} \tag{49}$$

where I_{cpi} and $c(x,y)$ represent correlation peak intensity and the correlation plane energy respectively. It shows the amount of power that shows up in the correlation peak.

4.3.1 PSR /PCE Ratios for Different SLM Size

In this section, we investigate effects of varying SLM size on the performance of a JTC. Figure 4-12 and Figure 4-13 presents the computer simulation results of PSR and PCE when the size of SLM is varied while the size of the joint image remain constant. The target and reference image are combined and zero padded to form a constant joint input image of size 64 x 64 pixels.

Figure 4-12: PSR Vs SLM Size

Figure 4-13: PCE Vs SLM Size

It can be seen that PSR increases with an increase in SLM size. A large SLM size allows the images to be spaced more reducing the possibilities of overlaps thus a better correlation output. Using a large SLM enables a higher dispersion of the phased pixels.

(a)

(b)

Figure 4-14: Correlation Output Using Different SLM Size But Same Joint Input Image (a)128 x 128 (b) 256 x 256

(a)

(b)

Figure 4-15: Correlation Output Using Different SLM Size But Same Joint Input Image (a)512 x 512 (b) 1024 x 1024

The correction peaks of Figure 4-15 (b) is much sharper and higher than that of the Figure 4-14 (a), indicating that a better performance is achieved with an increase in SLM size. The same results are deduced by the graphs in Figure 4-16 and Figure 4-17 where the PSR and PCE both increased as the size of the SLM were increased. Larger correlation plane (1024 x 1024 as opposed to 128 x 128) yields better results, with this in mind we look at the performance of different SLM sizes and joint input images while maintaining the ratio of joint input image to SLM size the same.

4.3.2 PSR /PCE for varying SLM Size and Varying Joint Input Image

Figure 4-18: PCE Vs Ratio of Joint Image to SLM Size

Figure 4-19: PSR Vs Ratio of Joint Image to SLM Size

In this section, we compare the performance of the JTC, when both joint input image and SLM size are varied and the ratio between them remains the constant. For simulation, we used the following ratios 16 x 16 / 128 x 128, 32 x 32 / 512 x 512, 64 x 64 / 1024 x 1024.

(a)

(b)

Figure 4-20: Correlation Output Using Different SLM Size and Joint Input Image Size but Same Image to SLM Size Ratio (a)16 x 16 / 128 x 128 (b) 32 x 32 / 256 x 256

(a)

(b)

Figure 4-21: Correlation Output Using Different SLM Size and Joint Input Image Size but Same Image to SLM Size Ratio (a)64 x 64 / 512 x 512 (b) 128 x 128 / 1024 x 1024

Although the ratio of the joint image to SLM size remains the same, we notice that there is a slight improvement on both PSR and PCE. This is mainly due to the fact that increase in image size and SLM size results in an increase in the number of pixels representing the actual image.

An increase in size and complexity of the joint image and SLM needed more computational power during the simulation and it took more time to attain the results.

4.3.3 PSR /PCE for varying No of Input Images

In this experiment, overlapping reference images are added to the SLM as the correlation intensity output is recorded. In the practical system, each reference image will be multiplied by a different orthogonal phase in prior and stored in the digital system. This process does not affect the overall performance of JTC. To simulate, a 'Rose' image of size 32 x 32 pixels is used as a reference image and as well as a test image while SLM size is selected as 256 x 256 pixels.

As the plots of performance metrics against the number of images show in Figure 4-22 and Figure 4-23, the proposed system performed better than the multi-reference phase encoded JTC. We can also note that as the number of reference images increased the difference in performance between the two decreased drastically and both systems performance decreased with an increase of images.

Figure 4-22: PSR Vs No of Images

Figure 4-23: PCE Vs No of Images

PSR = 180.1249
PCE = 196.77e-016

Figure 4-24: Correlation Output - One Reference Image

PSR = 61.2094
PCE= 15.177e-016

Figure 4-25: Correlation Output – Two Reference Images

PSR = 25.4667
PCE= 2.7654e-016

Figure 4-26: Correlation Output – Three Reference Images

PSR = 11.3467
PCE= 0.68181e-016

Figure 4-27: Correlation Output – Four Reference Images

Figure 4.24 to Figure 4.27 show the simulated plane for multiple inputs. The discrimination ability of the JTC decreases drastically after more than two reference images are used. This suggests

that, an increase in the number of input images results in higher side lobes, increasing distortion and thus affecting the PSR and PCE. The output at Figure 4-24 consists of more correlation inputs than expressed in the equation (4), which is represented Figure 4-19, but the results remain similar except that the correlation peak height is lower, an indication of lower PSR.

In theory, a JTC will produce correlation output regardless of the number of inputs, but from the simulated number of images we can infer that the discrimination abilities, correlation plane PSR are severely diminished when the total optical energy is increased relative to the reference image's energy. Figure 4.20 to Figure 4.24 show the decrease of correlation peak height as more reference images are included.

4.4 SPATIALLY EFFICIENCY EVALUATION

To investigate the effects of multiplexing reference images on the correlation output, we compare the output correlation peak while varying the number of reference images used. In all cases (see bottom row of each figure), multiplexed images setup gave a better correlation output.

4.4.1 Comparison of Correlation Outputs

Below we present a detailed study of the performance of the JTC in terms of correlation intensity, peak height and PSR when reference images are multiplexed and when they are placed side by used (spread mode). Here two kind of reference images are used: a Rose image and the image of Lena.

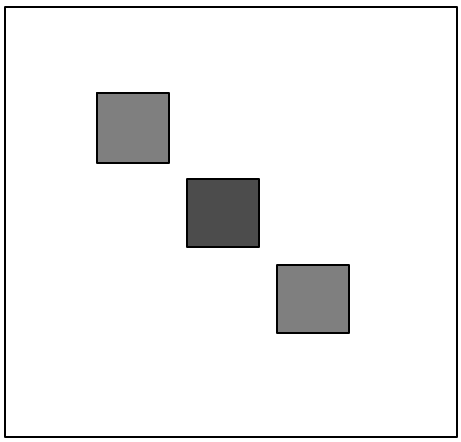

(a)Reference images placed side by side

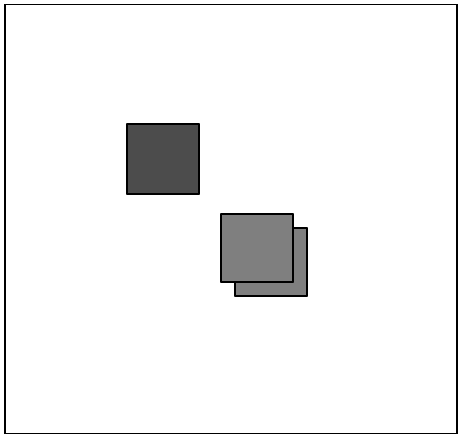

(b) Multiplexed reference images

(e)Image 1 Correlation PSR=91.5282

(f)Image 1 Correlation PSR=81.4571

(i)Image 2 Correlation (j)Image 2 Correlation

Figure 4-28: Correlations Outputs of Multplexed and Spread Images

By setting up a system identical with the previous and presenting the results side by side, we are able to assess the influence of the phase-only enhancement and the overlapping method.
In Figure 4-23, the performance of the modified phase JTC using a matched filter is presented and compared to the previous phase JTC with reference images placed in different ways. The multiplexing technique is found to yield good correlation output.

The simulation results shown in the previous section clearly show that the proposed method increased efficiency and the discrimination power of the conventional phase joint phase transform correlator. The result also demonstrates that known Pseudo-random sequences can be an alternative solution for creating phase masks while phase only information image is a good replacement of a complete image. The phase only correlation transformation had a significant increase on the image discrimination ability since the correlation spot size became smaller while correlation intensity height increased, thus increasing the JTC performance (accuracy increased).

5 CONCLUSION

This thesis started by briefly introducing optical processing in the initial chapters and summarizing its advantages over ordinary electronic processing as: high degree of parallelism, high overall processing speed, real time, design Complexity, independence of interference and energy efficiency. As a preliminary to the discussion of various architectures of optical correlation, the basic components being the spatial light modulator (SLM), charged coupled device (CCD), light source, mirrors, lenses and beam splitter are described in the second section. In the same section, the advantages and disadvantages of the two commonly used optical correlation techniques, the matched spatial filtering and the joint transform correlation, are listed. The section then proceeds to present the techniques that have been employed to improve on the performance of the JTC. The techniques include Fourier plane image subtraction, binarization, fringe adjusting and phase encoding input technique.

For better evaluation, mathematical expressions and architectural design of all the techniques mentioned above are included in section three. Another technique that was discussed and evaluate in chapter four was the multi-reference phase encoding input techniques.The analysis of maximum length sequences (M-sequences) which are linear, periodic Pseudo-random sequences that are generated by series of shift registers is included in section three. In this section image histogram plots and correlation output of a phase encoded JTC are used to compare different encoding levels (2, 3 and 5) used in the M-sequences to create different phase masks.

In chapter four, the proposed multi-reference phase encoded input JTC using phase SLM only is presented, analyzed and its correlation output compared to phased encode input JTC. Other

characteristics evaluation like spectral efficiency, PSR, PCE due to change in SLM size or joint image size are outlined in this section.

In summary the thesis, we presents a modified Multi-reference phase encoded input optical Joint Transform Correlator that is capable of exploiting the inherent massive connectivity and high processing speed of optics as well as spread spectrum capabilities of an M-sequence. One of the goals of designing the proposed system was to reduce the size of the optical setup; other aspects that were optimized are flexibility, robustness and simple implementation

For future research, we recommend a more detailed study on how the technique could be used in applications requiring multi-dimensional analysis (images with multi-dimensional data) enabling multi-dimensional image correlation. Another recommended study would involve the statistical capacity of the multiplex reference images on the SLM.

6 REFERENCES

[1] D. L. Flannery and J. L. Horner, "Fourier Optical Processors," Proc of IEEE, Vol. 77, No. 10, pp. 1511-1527, 1989.

[2] V. Lugt, "A Signal Detection by Complex Spatial Filtering," IEEE Tran. Inf. Theory, Vol. 10, pp. 139-145, 1964.

[3] C. S. Weaver and J. W. Goodman, "A Technique for Optically Convolving Two Functions," Applied Optics, 5, pp. 1248-1249, 1966.

[4] F. T. S. Yu and D. A. Gregory, "Optical Pattern Recognition: Architectures and Techniques," Proc of IEEE. 84, pp. 733-752, 1996.

[5] B. Javidi and C. Kuo, "Joint Transform Image Correlation using a Binary Spatial light Modulator at Fourier plane," Applied Optics, 27, pp. 663-665, 1988.

[6] M. S. Alam, O. Perez, and M. A. Karim, "Improved Correlation Discrimination using an Amplitude-Modulated Phase-Only Filter for Optimum Recognition," Applied Optics, 29, pp. 233-236, 1990.

[7] Q. Tang and B. Javidi, "Multiple-Object Detection with Chirp-Encoded Joint Transform Correlator," Applied Optics, 32, pp. 5079-5088, 1993.

[8] M. S. Alam and M. A. Karim, "Fringe-Adjusted Joint Transform Correlation," Applied Optics, 32, pp. 4344-4350, 1993.

[9] S. Thong, J. Jiang, and C. Li, "Joint Wavelet Transform Correlator with Power Spectrum Subtraction for Improved Performance," Optical Eng36, pp. 2787-2792, 1997.

[10] A. K. Cheri and M. S. Alam, "Reference Phase-Encoded Fringe-Adjusted Joint Transform Correlation," Applied Optics, Vol 40, No 8, 2001.

[11] G. Lu, Z. Zhang, and F. T. S. Yu, "Phase Encoded Input Joint Transform with improved Pattern Discriminability," Opt. Letter. 20, 1307-1309, 1995.

[12] A. Alsamman, PhD Thesis.

[13] D. G. Feitelson, "Optical Computing: A Survey for Computer Scientists," Cambridge, MA, the MIT Press, 1988.

[14] D. McGloin, G. C. Spadling, H. Melville, W. Sibbette and K. Dholakia, "Application of Spatial Light Modulators in Atom Optics," Optics Express, Vol. 11, No. 2, 2003.

[15] B. G. Boone, "Signal Processing using Optics: Fundamentals, Devices, Architectures and Applications," Oxford, New York, 1998.

[16] L. Yaroslavyky, "Digital Image Processing: Application," Course 0510.7211 Notes, Semester B, Tel Aviv University, 2005.

[17] A. C. Davenhall, G. J. Privett and M. B. Taylor, "The 2-D CCD Data Reduction Cookbook," Starlink Cookbook 5, 2001. http://www.starlink.rl.ac.uk/star/docs/sc5.htx/sc5.html.

[18] T. P. Cheatham, Jr. and A. Kohlenberg, "Optical Filters: Their Equivalence to and Differences from Electrical Networks, IRE Convention Record, pt. 4, pp. 6-12, 1954.

[19] C. Hendrix and B. Kumar, "Design and Testing of 3-Level Optimal Correlation Filters," Proc. SPIE, Vol 1564, Optical Inf. Proc. Sys, pp. 2-12, 1991.

[20] V. Lugt, "The Effects of Small Displacements of Spatial Filters," Applied Optics, 6, pp. 1221-1225, 1967.

[21] L. Cai, Y. Jin, S. Zhou, P. Yeh, N. Marzwell and H. Liu, "Translational Sensitivity Adjustable Compact Optical Correlator and its Application for Fingerprint Recognition," Opt. Eng. 35, pp. 415-422, 1996.

[22] M. Montes-Usategui, S.E. Monroe and R.D. Juday, "Automated Self-Alignment Procedure for Optical Correlators," Opt. Eng. 36, pp.1782-1791, 1997.

[23] J. A. Davis, M.A. Waring, G.W. Bach, R.A. Lilly and D.M. Cottrell, "Compact Optical Correlator Design," Applied Optics. 28, pp. 10-11, 1989.

[24] I. Juvells, S. Vallmitjana and S. Bosch, "Analysis of a Scale Tunable Telephoto Lens and its use in Optical Correlation," J. Modern Optics. 39, pp. 1107-1115, 1992.

[25] B. Javidi, C .J. Kuo and S. F. Odeh, "Comparison of Bipolar Joint Transform Image Correlator and Phase Only Matched Filter Correlators," Proc SPIE 938, pp. 66-76, 1988.

[26] B. Javidi and C. Kuo, "Joint Transform Image Correlation using a Binary Spatial light Modulator at Fourier plane," Applied Optics. 27, pp. 663-665, 1988.

[27] A.V. Oppenheim and J. S. Lim, "The Importance of Phase in Signals," Proceedings of the IEEE. 69, pp. 529–541, 1981.

[29] A. Glen, "On the Period Length of Pseudo-random Number Sequences," University of Adelaide, Australia, Nov 2002.

[31] N. Zierler, "Linear Recurring Sequences," J. Soc Indust Appl Math 7, pp. 31-49,1959.

[32] S. W. Golomb, "Shift Register Sequences," Aegean Park Press, Lagun Hills, CA 1982

[33] J. J. Rushanan, "A Tutorial on Finite Fields and Binary M-sequences," Dec 1996, Mitre Corporation.

[34] F. J. Mac Williams and N. J. A Sloane, “Pseudo-random Sequences and Arrays,” Proc Inst Elec. Eng, Vol. 64, No12, pp. 1715-1729, 1976.

[35] D. H. Green, “Structural Properties of Pseudo-random Arrays and Volumes and Their Related Sequence,” IEEE Proc, Vol 132, Part E, No .3 pp. 133-145, 1985.

[36] C. J. Kuo, H. B. Rigas, “Quasi M-arrays and Gold Code Arrays,” IEEE Trans on Information Theory, Vol 37, No 2, pp. 385-388, 1991.

[37] A.Alsamman, “Spatially Efficient Pseudo-random Encoded JTC for Fast Target Recognition”, Proc of SPIE Vol. 5816,pp. 252-257,2005.

[38] B. Javidi and J. L. Horner, “Optical Pattern Recognition for Validation and Security Verification”, Optical Engineering 33, 1752-1756, 1994.

[39] T. X. Matoba, T Shimura, Kuroda and B. Javidi, “ Secure Optical Storage that uses Fully Phase Encryption”, Applied Optics 39, 6689-6694, 2000.

7 VITA

Edward Mwatibo was born in Voi, Kenya and received his Bachelors of Technology degree in Electrical and communication from Moi University –Eldoret in 1993.